Data Repository Item 2009117

Appendix: Luminescence methodology

Sampling and sample preparation

Samples were collected by hammering a steel tube in the loose sediment and emptying the tube into opaque plastic bags. See Fig. DR1 and DR2 as examples for sampling sites. The samples were processed using standard methods, i.e. sieving, chemical treatment, density separation using LST Fastfloat and quartz etching with concentrated (40%) HF (Mejdahl, 1985). Either 100-150 µm or 150-200 µm fractions were isolated (Table DR1). The potassium-rich feldspar separates were obtained by density separation in LST Fastfloat (ρ = 2.58 g cm^{-3}). No HF acid etching was used in the feldspar preparation because this will most probably not remove a uniform layer from the feldspar grains (Duller, 1992) and an a-value of 0.07 ± 0.02 was assumed (Preusser, 1999). Quartz was extracted using densities of 2.58 and 2.70 g cm^{-3}. Feldspar contaminated quartz samples were additionally treated in hydrofluorosilicic acid (H_2SiF_6) for one week.

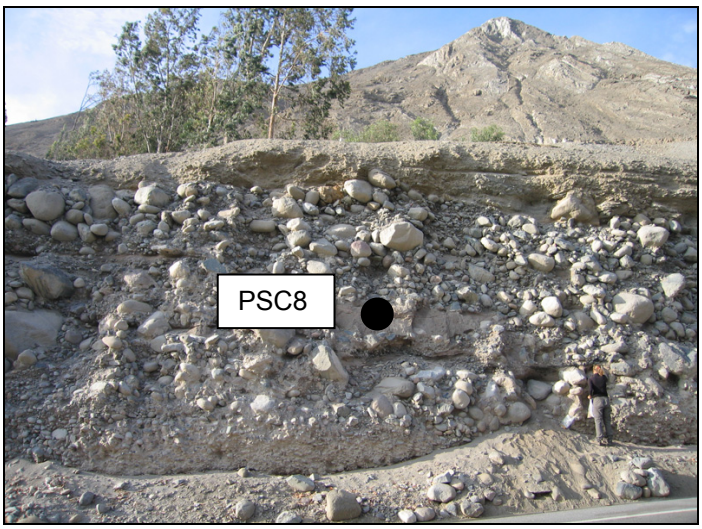

Figure DR1: Example for sampling location of sample PSC8 in the conglomerates of the fluvial terraces. These deposits are located just below the knickzone where the sorting of the components is very bad (see main text for more information).The sand lens in the middle of the photograph was sampled. See person on the lower right for scale.

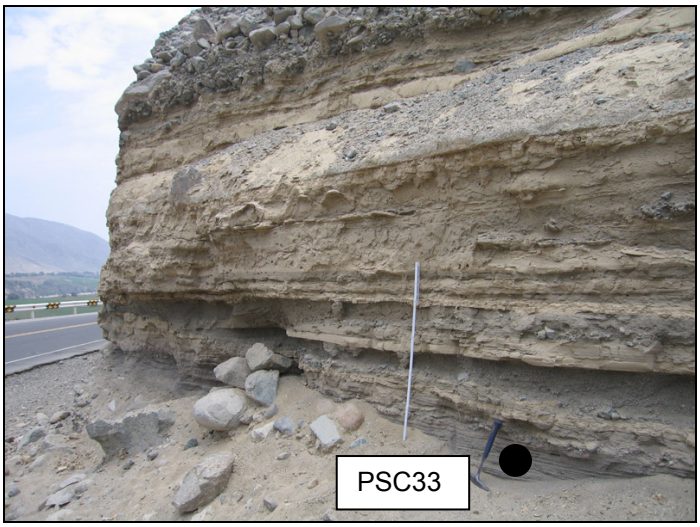

Figure DR2: Sample location of sample PSC33. White stick is one meter in size. These sand layers with a breccia on top are clearly fluvial deposits and are very well bleached (Table DR1).

Measurement setup

Infrared stimulated luminescence (IRSL) was measured using a Risø DA-20 TL/OSL reader, fitted with an internal $^{90}Sr/^{90}Y$ beta-source. Photons were filtered through a combination of a Schott BG39 and an interference filter, resulting in a maximum peak at 410 nm, and effectively removing the UV light. This is important because detection of feldspar emission by a conventional U340 filter includes the thermally unstable emission waveband of 280 to 290 nm, which may cause significant age underestimation (Krbetschek et al., 1997). Feldspar was stimulated using infrared LEDs (870 nm) with an intensity of 108 $mWcm^{-2}$. Quartz luminescence was stimulated with blue diodes (470 ± 30 nm) and an intensity of 34 $mWcm^{-2}$ and the emitted photons were filtered using a UV340 filter.

Grains were mounted on stainless steel discs using silicone spray resulting in a monolayer of grains. Typically a 4 mm diameter was used, resulting in approximately 400 grains per aliquot. The signal was integrated from the first second of stimulation, minus a background estimated from the last 25 s of a total of 300 s stimulation. The equivalent dose (D_e) from feldspar was identified as being independent of the initial signal integration time. All aliquots with a recycling ratio that was not within 10% of unity were excluded from further analysis. A machine error of 1.5% was assumed.

Quartz OSL vs. feldspar IRSL ages

The potassium-rich feldspar extracts were carefully tested with a preheat plateau test on selected samples and a dose recovery test on all samples (Fig. DR3 and DR4). All samples behaved very nicely in the dose recovery tests. For some samples the preheat plateau test did not show a distinct plateau because of the big spread in D_e among the different aliquots.

Nevertheless, we were able to determine preheat plateaus from some samples. Based on these tests, IRSL was measured using a 250°C preheat for 10 s and a cutheat to 210°C.

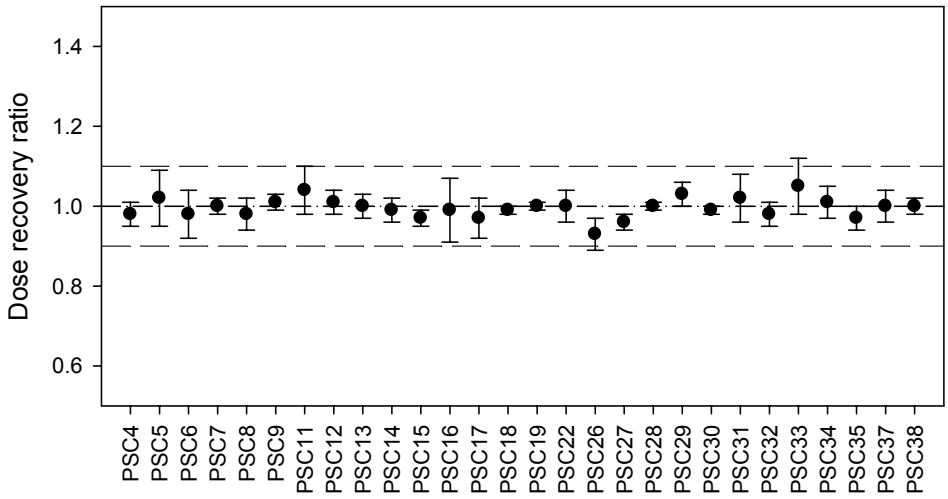

Figure DR3: Dose recovery ratio for the feldspar samples. This test shows if it is possible to recover a known dose. A value of 1 means that the recovered dose and the given dose are identical.

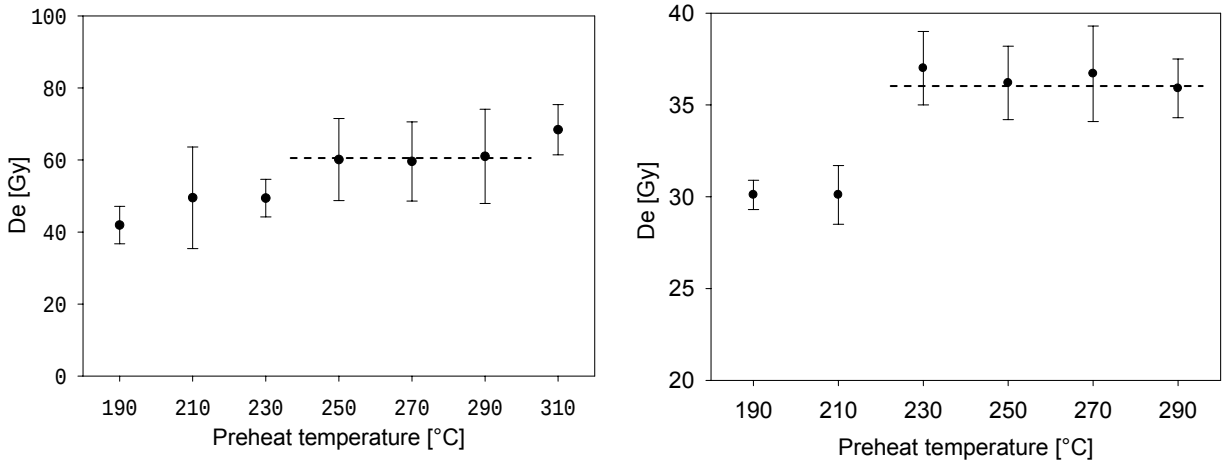

Figure DR4: Preheat plateau test for sample PSC15 and PSC32. Note that the preheat temperature was varied while the cutheat temperature was kept constant at 210°C. The preheat plateau of sample PSC15 goes from 250°C to 290°C and for PSC32 from 230°C to 290°C. Based on such tests from selected samples, a preheat temperature of 250°C and a cutheat at 210°C were applied for D_e determination.

Comparison of quartz with feldspar ages revealed a systematic underestimation of the quartz ages, with only 11 out of 28 samples being in agreement. Extended testing on the quartz

extracts that underestimate the corresponding IRSL age revealed that the medium component of the OSL signal from the regenerated dose is higher relative to the fast component than in the natural OSL signal. Thermal stability measurements of the medium component confirmed that this component is thermally very unstable, and where it is not present in the natural signal, causes an age underestimation (Steffen, 2008). As a solution to this problem, we extracted the fast component by curve fitting and calculated the D_e based on the fast component only. Using this approach, we could reproduce the corresponding IRSL age. This can be used as a further support of the IRSL ages and also shows that the quartz optically stimulated luminescence (OSL) age underestimates the true age due to a contamination of the fast component by an unstable medium component. For more information on this issue see Li and Li (2006).

Dose rate calculation

Dose rates were calculated from U, Th, and K contents measured using high-resolution gamma spectrometry (Table DR3). Note that the dose rate is calculated from sediment surrounding the IRSL sample. While for most samples there is a minimum of 30 cm radius sphere of homogenous sediment around the sampling position, there are also sampling sites where the sand layer is less than 30 cm thick. For these samples, we modeled the influence of the layers above and below the sampling site on the gamma dose rate with ADELE software (Kulig, 2005) by varying the values for U, Th and K. Note that the values most probably don't vary much as thin sand layers (< 30 cm) were only sampled on alluvial fans where the bedrock geology in the catchment is uniform. From this modeling, it is concluded that dose rates for these particular samples vary by a maximum of 5% due to gamma irradiation from surrounding layers. Based on the results from high-resolution gamma spectrometry, we can also exclude significant disequilibrium in the uranium decay series.

Cosmic dose rates were calculated using present day values for sediment overburden. Note that changes in overburden only affect the total dose rate marginally. While the total dose rate is, for most of the samples, between 3 – 4 Gy/ka, the contribution of the cosmic radiation is only about 0.1 Gy/ka and varies for about 0.05 Gy/ka when extreme changes in sediment overburden are assumed. Nevertheless, changes in sediment overburden can be accounted for introducing an uncertainty of 10% into the cosmic dose rate calculation.

Although the samples are now completely dry, it cannot be excluded that during wet periods, there was a certain amount of water in the sediment. Comparable samples from an alluvial fan in Switzerland indicate a water content of about 6%. This value fits well into other water content measurements on similar sample material and we therefore assume this as a maximum value for our samples in the Pisco valley during wet periods. Because the wet periods make up about 50% of the last 55 ka we assume a water content of 0-6% during the whole time. Note that these periods with varying water content were additionally modelled with ADELE software (Kulig, 2005). In conclusion, water content was assumed to be 3 ± 3%.

Dose distribution – D_e extraction

Calculation of D_e from the individual aliquot measurements was done using various statistical approaches. This is important because fluvial samples may be incompletely bleached prior to deposition (Fig. DR5). For all samples, D_e was calculated using the median, central age model (CAM), minimum age model (MAM) and finite mixture model (FMM, Galbraith and Green, 1990; Galbraith et al., 1999). For about two thirds of the samples, all of the models gave identical results. Discrimination between use of the CAM and FMM (MAM) was done using a decision process for single aliquots similar to the one proposed by Arnold et al. (2007). This was modified by stipulating an overdispersion of >15% in order to discard the CAM. It is interesting to note that in all samples where the decision process favored the CAM, the FMM could not be applied due to an overfit. The results from the MAM and FMM are generally identical. Following the suggestions by Rodnight et al. (2006), the FMM was used for all the samples where the CAM was inappropriate. Where the lowest component in the FMM included less than 10% of the grains, this component was disregarded and the next youngest component was used for the calculation of D_e. We are aware that the number of measured aliquots (~30 aliquots) per sample is on the low side for fluvial deposits. However, it was shown by Spencer and Robinson (2008) in a similar setting that this number of measured aliquots was able to provide accurate ages.

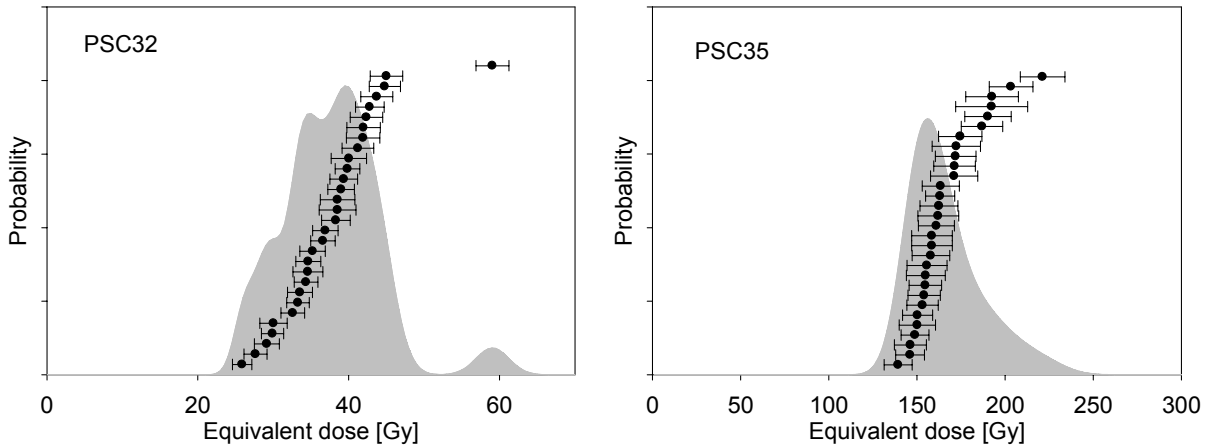

Figure DR5: Probability density function for sample PSC32 and PSC35. Sample PSC32 was extracted from a thin sand layer on an alluvial fan, which was most probably deposited by secondary processes on the alluvial fan. PSC35 originates from fluvial terrace deposits relatively close to the outlet of the basin (Table DR1). Note that the sample PSC35 is much better bleached than sample PSC32. This is not surprising, as the transport distance, and hence the bleaching probability, is much higher for sample PSC35. Nevertheless, the D_e *extracted from the dose distribution of sample PSC32 using the FMM matches the radiocarbon age of that deposit.*

Fading tests

IRSL dating of feldspar from some regions seems to systematically underestimate the known age of a sample due to anomalous fading of the luminescence signal (e.g. Huntley and Lamothe, 2001). However there are several studies showing that feldspar is able to yield ages that are in good agreement with independent age control (e.g. Berger et al., 2004; Juschus et al., 2007; Preusser, 2003; Vandergoes et al., 2005). It has been proposed that it is possible to detect and correct for anomalous fading (e.g. Huntley and Lamothe, 2001; Lamothe et al., 2003). However, the proposed correction method is only applicable for the linear part of the growth curve, limiting its use to young samples (i.e. Holocene). Concerning the samples from the Pisco valley, there is evidence that they are not, or only slightly, affected by anomalous fading (Table DR2). Independent age control from wood (radiocarbon) from within sample PSC32 shows similar results to the IRSL age, although the IRSL slightly underestimates the calibrated radiocarbon age (radiocarbon: 10.6 ± 0.2 ka, IRSL: 9.1 ± 0.9 ka). The radiocarbon age was measured at ETH Zurich (Lab no: ETH-32345, uncalibrated C14 age: 9350 ± 70 a BP). However, applying a fading correction using the g-value as proposed by Huntley and Lamothe (2001), results in an overestimation of the radiocarbon age (12.0 ± 1.1 ka). Fading tests using delayed L_x/T_x measurements on all samples show that the signal in most of the samples from the Pisco valley decreases by about 10% compared to measurements without any delay (average fading ratio after a delay of 167 days: 0.88 ± 0.05, exact numbers see Table DR2). However, this value does not depend on the storage time. Identical results were obtained for storage times of 4.5, 62 and 167 days (Table DR2), and this is in agreement with a study from Molodkov et al. (2007), where anomalous fading was avoided by storing the samples for a month, rather than preheating them. They suggested that at least part of the IRSL depletion is connected with tunneling processes in the early stages of relaxation, and that the characteristic time of attenuation for these processes is several days, after which they fall below a level that would result in a significant age underestimation. Therefore, the measured loss of signal is representative only of artificial laboratory irradiation, and cannot be projected into the geological past and used for naturally irradiated samples with a much lower environmental dose. However, this loss of signal has an influence, in that it overestimates the regenerated dose, and therefore the dose response curve, if there is not enough time between irradiation and measurement. It is therefore considered important to leave enough time between irradiation and measurements, where each measurement step is conducted on all aliquots before proceeding to the next step in the SAR protocol. We therefore believe that for these samples, most of the “apparent fading” can be accounted for by not using the “run one at a time” option in the measurement sequence and by using a filter combination that effectively removes the UV light.

References Cited

Arnold, L.J., Bailey, R.M., and Tucker, G.E., 2007, Statistical treatment of fluvial dose distribution from southern Colorado arroyo deposits: Quaternary Geochronology, v. 2, p. 162-167.

Berger, G.W., Melles, M., Banerjee, D., Murray, A.S., and Raab, A., 2004, Luminescence chronology of non-glacial sediments in Changeable Lake, Russian High Arctic, and implications for limited Eurasian ice-sheet extent during the LGM: Journal of Quaternary Science, v. 19, p. 513-523.

Duller, G.A.T., 1992, Luminescence chronology of raised marine terraces, south-west North Island, New Zealand: Unpublished Ph.D. thesis, University of Wales, Aberystwyth.

Galbraith, R.F., and Green, P.F., 1990, Estimating the component ages in a finite mixture: Nuclear Tracks and Radiation Measurements, v.17, p. 197-206.

Galbraith, R.F., Roberts, R.G., Laslett, G.M., Yoshida, H. and Olley, J.M., 1999, Optical dating of single and multiple grains of quartz from Jinmium rock shelter, northern Australia: Part I, experimental design and statistical models: Archeometry, v. 41, p. 339-364.

Huntley, D.J., and Lamothe, M., 2001, Ubiquity of anomalous fading in K-feldspars and the measurement and correction for it in optical dating: Canadian Journal of Earth Sciences, v. 38, p. 1093-1106.

Juschus, O., Preusser, F., Melles, M., and Radtke, U., 2007, Applying SAR-IRSL methodology for dating fine-grained sediments from Lake El'gygytgyn, north-eastern Siberia: Quaternary Geochronology, v. 2, p. 187-194.

Krbetschek, M.R., Götze, J., Dietrich, A., and Trautmann, T., 1997, Spectral information from minerals relevant for luminescence dating: Radiation Measurements, v. 27, p. 695-748.

Kulig, G., 2005, Erstellung einer Auswertesoftware zur Altersbestimmung mittels Lumineszenzverfahren unter spezieller Berücksichtigung des Einflusses radioaktiver Ungleichgewichte in der 238U-Zerfallsreihe: Unpublished BSc thesis, Technical University Bergakademie Freiberg.

Lamothe, M., Auclair, M., Hamzaoui, C., and Huot, S., 2003, Towards a prediction of long-term anomalous fading of feldspar IRSL: Radiation Measurements, v. 37, p. 493-498.

Li, B., and Li, S.-H., 2006, Comparison of D_e estimates using the fast component and the medium component of quartz OSL: Radiation Measurements, v. 41, p. 125-136.

Mejdahl, V., 1985, Thermoluminescence dating of partially bleached sediments: Nuclear Tracks and Radiation Measurements, v. 10, p. 711-715.

Molodkov, A., Jaek, I., and Vasilchenko, V., 2007, Anomalous fading of IR-stimulated luminescence from feldspar minerals: some results of the study: Geochronometria, v. 26, p. 11-17.

Preusser, F., 1999, Lumineszenzdatierungen fluviatiler Sedimente – Fallbeispiele aus der Schweiz und Norddeutschland: Kölner Forum für Geologie und Paläontologie, v. 3, 63 p.

Preusser, F., 2003, IRSL dating of K-rich feldspars using the SAR protocol: Comparison with independent age control: Ancient TL, v. 21, p. 17-23.

Rodnight, H., Duller, G.A.T., Wintle, A.G., and Tooth, S., 2006, Assessing the reproducibility and accuracy of optical dating of fluvial deposits: Quaternary Geochronology, v. 1, p. 109-120.

Spencer,J.Q.G., and Robinson, R.A.J., 2008, Dating intramontane alluvial deposits from NW Argentina using luminescence techniques: Problems and potential: Geomorphology, v. 93, p. 144-155.

Steffen, D., 2008, Late Quaternary sediment aggradation and erosion in the Pisco and Majes valleys in southern Peru: the role of climatic variations [Ph.D. thesis]: University of Bern, 92 p.

Vandergoes, M.J., Newnham, R.M., Preusser, F., Hendy, C.H., Lowell, T.V., Fitzsimons, S.J., Hogg, A.G., Kasper, H.U., and Schlüchter, C., 2005, Regional insolation forcing of late Quaternary climate change in the Southern Hemisphere: Nature, v. 436, p. 242-245.

Table DR1: *Full details of the luminescence samples analytics*

Sample	*Grain size*	*n**	σ_{OD}	skew[#]	*Dose rate*	D_e	*Age*	*Age*	*Prop.*	*Location*[##]		*Altitude*	*Terrace*
	(µm)		*(%)*[§]		*(Gy/ka)*	*(Gy)*	*(ka)*	*model* **	*(%)*[§§]	*Easting*	*Northing*	*(m asl)*	*level*
PSC4	149-208	30	6.3	0.65	4.89±0.25	241.53±4.14	**49.4±2.8**	FMM	93	461278	8497770	2421	1
PSC5	149-208	31	16.0	1.34	4.27±0.22	118.57±3.03	**27.8±1.6**	FMM	84	455252	8495708	2058	2
PSC6	149-208	30	6.6	0.10	4.39±0.22	99.31±1.46	**22.6±1.3**	CAM		453808	8495618	1955	2
PSC7	149-208	24	49.9	0.40	1.97±0.11	23.01±1.23	**11.7±0.9**	FMM	39	451304	8495996	1774	3
PSC8	100-150	30	29.5	1.01	3.71±0.20	141.91±4.11	**38.2±2.5**	FMM	72	443385	8500462	1347	1
PSC9	104-149	30	18.9	2.37	3.90±0.21	104.92±2.28	**26.9±1.7**	FMM	96	442078	8500482	1242	2
PSC11	149-208	29	21.5	1.01	3.44±0.17	134.80±8.97	**39.2±3.3**	FMM	39	436259	8497264	1057	1
PSC12	149-208	29	13.2	1.41	2.28±0.13	104.51±2.56	**45.8±2.9**	FMM	96	436259	8497264	1057	1
PSC13	149-208	30	19.5	0.09	3.79±0.19	84.49±5.88	**22.3±2.0**	FMM	15	436087	8496980	1073	2
PSC14	149-208	30	22.3	2.71	3.60±0.18	17.62±0.39	**4.9±0.3**	FMM	90	436127	8497194	1068	3
PSC15	149-208	30	11.9	1.58	2.22±0.12	58.80±1.40	**26.5±1.6**	FMM	91	436100	8497332	1133	2
PSC16	149-208	30	10.1	0.26	3.59±0.17	35.14±0.87	**9.8±0.6**	FMM	74	435068	8496964	1041	3
PSC17	149-208	28	13.2	0.17	3.63±0.18	90.85±2.70	**25.0±1.5**	FMM	20	435020	8496934	1036	2
PSC18	100-150	30	13.9	1.66	2.93±0.16	158.03±3.56	**54.0±3.5**	FMM	92	421224	8491924	798	1
PSC19	104-149	30	10.3	1.17	3.33±0.17	153.37±3.46	**46.0±3.0**	FMM	95	421166	8491970	815	1
PSC22	149-208	33	29.0	0.00	3.13±0.15	32.70±1.69	**10.2±0.8**	FMM	25	421399	8491980	781	1
PSC26	100-150	29	10.5	-0.06	3.21±0.18	165.88±4.10	**50.4±3.4**	CAM		421519	8491478	731	3
PSC27	100-150	30	23.7	0.79	3.44±0.18	61.51±2.09	**17.9±1.2**	FMM	55	421338	8491298	733	1
PSC28	149-208	30	27.6	-0.36	3.45±0.17	55.24±2.13	**16.0±1.1**	FMM	45	421256	8490974	738	2
PSC29	149-208	30	33.5	-0.27	3.89±0.19	28.75±1.57	**7.4±0.6**	FMM	28	421332	8491066	731	3
PSC30	104-149	29	16.1	0.91	2.95±0.15	153.18±4.79	**51.9±3.4**	FMM	83	414414	8488388	706	1
PSC31	104-149	30	17.2	0.87	2.99±0.15	103.44±9.82	**34.6±3.8**	FMM	15	414933	8488062	653	1
PSC32	149-208	30	16.1	0.87	3.45±0.17	31.44±2.52	**9.1±0.9**	FMM	31	414934	8488086	656	3
PSC33	100-150	30	5.2	-0.06	3.28±0.17	157.34±2.55	**48.0±2.9**	CAM		414865	8487756	607	1
PSC34	104-149	30	16.5	1.40	3.16±0.16	168.30±4.02	**53.3±3.2**	FMM	91	414990	8487802	608	1
PSC35	100-150	30	8.7	1.20	3.39±0.17	161.70±3.78	**47.7±2.9**	FMM	92	404577	8482228	446	1
PSC37	149-208	30	18.2	1.72	3.85±0.23	26.96±0.67	**7.0±0.5**	FMM	90	404621	8482726	405	3
PSC38	100-150	30	6.9	0.20	3.49±0.18	179.94±2.52	**51.5±2.9**	CAM		390153	8486196	245	1

* Number of measured aliquots
§ Overdispersion
# Skew of the dose distribution
** CAM = Central age model, FMM = Finite mixture model
§§ Proportion of aliquots included in the FMM age
Sample location in UTM 18S coordinates, datum: Provisional South American Datum 1956.

Table DR2: *Results of the fading tests using delayed L_x/T_x measurements.*

Sample	***10 min §,****	***7 hours****	***36 hours****	***4.5 days****	***62 days****	***167 days****	***167/4.5 days#***
PSC4	0.95±0.04	0.98±0.04	0.94±0.04	0.88±0.03	0.94±0.04	0.90±0.04	1.02±0.05
PSC5	1.01±0.05	0.96±0.05	0.90±0.05	0.83±0.05	0.87±0.06	0.84±0.05	1.02±0.07
PSC6	0.94±0.04	0.91±0.04	0.85±0.03	0.90±0.04	0.90±0.04	0.86±0.04	0.96±0.05
PSC7	0.98±0.08	0.95±0.09	0.90±0.08	0.85±0.07	0.84±0.08	0.79±0.08	0.93±0.11
PSC8	0.97±0.07			0.83±0.06	0.84±0.07	0.85±0.06	1.03±0.09
PSC9	1.00±0.05	1.00±0.05	0.92±0.04	0.84±0.04	0.91±0.05	0.83±0.05	0.99±0.06
PSC11	1.03±0.11			0.93±0.10	0.87±0.10	0.94±0.10	1.01±0.14
PSC12	0.97±0.08	0.90±0.08	0.86±0.08	0.79±0.07	0.85±0.08	0.79±0.07	0.99±0.10
PSC13	0.92±0.05			0.83±0.05	0.80±0.05	0.84±0.05	1.01±0.06
PSC14	0.97±0.05			0.83±0.04	0.83±0.05	0.87±0.05	1.06±0.06
PSC15	0.95±0.06	0.98±0.06	0.86±0.05	0.79±0.05	0.85±0.06	0.80±0.06	1.01±0.07
PSC16	0.96±0.09			0.87±0.08	0.83±0.09	0.92±0.09	1.05±0.12
PSC17	1.05±0.11	0.94±0.11	0.94±0.11	0.85±0.08	0.85±0.09	0.86±0.09	1.01±0.12
PSC18	0.97±0.05	0.93±0.05	0.88±0.04	0.83±0.04	0.89±0.05	0.85±0.05	1.02±0.06
PSC19	0.94±0.04	0.94±0.04	0.92±0.04	0.86±0.04	0.88±0.04	0.82±0.04	0.95±0.05
PSC22	0.98±0.04			0.84±0.04	0.81±0.04	0.88±0.04	1.04±0.05
PSC26	0.94±0.06			0.90±0.06	0.94±0.07	0.96±0.07	1.08±0.10
PSC27	0.95±0.04			0.86±0.04	0.89±0.05	0.87±0.05	1.00±0.06
PSC28	1.01±0.04			0.87±0.03	0.90±0.04	0.87±0.04	1.00±0.05
PSC29	1.00±0.05			0.90±0.04	0.86±0.05	0.90±0.05	1.00±0.06
PSC30	0.99±0.07			0.84±0.06	0.82±0.06	0.92±0.06	1.09±0.08
PSC31	1.00±0.07			0.88±0.06	0.88±0.07	0.96±0.07	1.10±0.09
PSC32	1.00±0.06			0.91±0.05	0.85±0.05	0.99±0.06	1.09±0.08
PSC33	1.01±0.07			0.88±0.06	0.82±0.06	0.89±0.06	1.01±0.08
PSC34	0.97±0.06			0.86±0.05	0.83±0.05	0.88±0.05	1.03±0.07
PSC35	1.00±0.07			0.87±0.06	0.88±0.06	0.91±0.06	1.05±0.08
PSC37	1.01±0.07			0.84±0.06	0.86±0.07	0.91±0.07	1.08±0.09
PSC38	0.98±0.04			0.86±0.04	0.85±0.04	0.84±0.04	0.98±0.05
Average	0.98±0.03	0.95±0.03	0.90±0.03	0.86±0.03	0.86±0.04	0.88±0.05	1.03±0.05

§ Opening of the lid and exposure to laboratory red light for 10 min
* Ratio of the signal measured after a storage time at room temperature compared to "immediate" measurements as in the SAR protocol. Note that in this case, "immediate" includes a delay of approximately 7 hours between irradiation and measurement.
# Ratio of 167 days to 4.5 days storage time

Table DR3: *Dose rate data including K, Th and U concentrations. Note that a 10 % uncertainty is applied to the cosmic dose rate*

Sample	Dose rate (Gy/ka)	Cosmic dose rate (mGy/ka)	K (%)	Th (ppm)	U (ppm)
PSC4	4.89±0.25	16	2.76±0.06	13.07±0.83	2.81±0.11
PSC5	4.27±0.22	35	2.27±0.05	11.12±0.54	2.61±0.11
PSC6	4.39±0.22	146	2.05±0.04	13.44±0.87	2.90±0.11
PSC7	1.97±0.11	151	0.85±0.02	2.82±0.14	0.73±0.03
PSC8	3.71±0.20	72	1.84±0.04	10.06±0.52	2.63±0.15
PSC9	3.90±0.21	88	1.91±0.04	11.41±0.56	2.66±0.16
PSC11	3.44±0.17	30	1.77±0.04	8.12±0.40	2.09±0.09
PSC12	2.28±0.13	10	1.04±0.02	4.04±0.30	1.13±0.05
PSC13	3.79±0.19	130	1.90±0.04	9.05±0.63	2.37±0.10
PSC14	3.60±0.18	132	0.97±0.02	13.13±0.65	3.83±0.14
PSC15	2.22±0.12	130	0.89±0.02	4.21±0.31	1.25±0.05
PSC16	3.59±0.17	168	1.61±0.03	8.67±0.43	2.55±0.11
PSC17	3.63±0.18	82	1.58±0.03	10.20±0.48	2.82±0.11
PSC18	2.93±0.16	22	1.49±0.03	8.38±0.63	1.57±0.07
PSC19	3.33±0.17	143	1.53±0.03	9.10±0.68	2.30±0.08
PSC22	3.13±0.15	175	1.63±0.03	6.28±0.31	1.60±0.06
PSC26	3.21±0.18	21	1.37±0.03	11.03±0.65	2.65±0.12
PSC27	3.44±0.18	80	1.60±0.03	9.94±0.63	2.46±0.10
PSC28	3.45±0.17	214	1.46±0.03	9.51±0.47	2.19±0.10
PSC29	3.89±0.19	208	1.53±0.03	12.32±0.58	2.83±0.11
PSC30	2.95±0.15	15	1.37±0.03	7.35±0.36	2.42±0.10
PSC31	2.99±0.15	28	1.59±0.03	6.80±0.41	1.87±0.08
PSC32	3.45±0.17	136	1.57±0.03	8.08±0.47	2.49±0.09
PSC33	3.28±0.17	28	1.63±0.03	9.01±0.60	2.19±0.09
PSC34	3.16±0.16	40	1.49±0.03	7.71±0.37	2.59±0.09
PSC35	3.39±0.17	94	1.81±0.04	7.67±0.41	2.10±0.09
PSC37	3.85±0.23	155	1.73±0.04	9.17±0.53	2.73±0.58
PSC38	3.49±0.18	132	1.91±0.04	6.62±0.34	2.40±0.09

.